PORE NETWORK MODELS TO CALCULATE TRANSPORT AND ELECTRICAL PROPERTIES OF SINGLE OR DUAL-POROSITY ROCKS

S. Békri, C.Laroche, O. Vizika
Institut Français du Pétrole, 1 et 4 avenue de Bois-Préau, 92852 Rueil-Malmaison, France

This paper was prepared for presentation at the International Symposium of the Society of Core Analysts held in Toronto, 21-25 August 2005

ABSTRACT

The objective of the present work is to demonstrate the effect of pore structure on fluid transport and electrical properties of homogeneous or dual-porosity pore structures for drainage conditions. To this end, a pore network numerical simulator is used that calculates multiphase flow and electrical properties taking into account the pore structure specificities. The characteristics of the 3-D pore-network are defined with the requirement that it satisfactorily reproduces the capillary pressure curve, the porosity and the permeability values which were determined experimentally. Gas/oil transport properties are calculated and compared to experimentally determined curves. The simulations show that different input parameters can lead to similarly good reproductions of the experimental capillary pressure. However, only representative network of the real media, in terms of coordination number and average pore radius, gives a good agreement with the measured relative permeabilities. The quantitative effect of pore structure on transport and electrical properties in homogeneous (Fontainebleau) sandstone is demonstrated. The so-called "non-Archie" behavior is confirmed at low water saturation. It is found that the resistivity index and saturation exponent are greatly affected by the pore shape factor (λ_p) and the wettability.

INTRODUCTION

The microscopic pore space structure of a porous medium controls the fluid transport and the electrical characteristics of the reservoir rocks. However, the exact solution of the pore scale equations is difficult to obtain, due to the complexity of the real pore space of porous media. Research efforts have focused on ways to simplify the three-dimensional irregular pore system. The simplified equivalent "pore network model", which can be mathematically treated, can take into account essential features of the pore space geometry and topology. The pore networks are flexible models that can account for different phenomena occurring at the pore scale. They permit the calculation of different petrophysical parameters relevant for single phase or multiphase flow (e.g. absolute permeability, relative permeabilities of fluids, formation factor, electrical resistivity index, etc.). Significative efforts have been made for the prediction of macroscopic transport coefficients of the reservoir rocks using pore network models. An extended review of most of these models is given by Sahimi [13]. Several authors have also looked at the

electrical properties of partially water-saturated porous rocks using pore network models. Dicker and Bemelans [3] used networks of cylindrical pores and found that the coordination number and the width of the pore-size distribution affect the saturation exponent. Wang and Sharma [16] found that high network connectivities result in relatively low values of saturation exponent for both water-wet and oil-wet pore network. Man and Jing [10] stressed the importance of the pore shape to simulate the so-called "non-Archie" behavior in low saturations. They have found that the use of more realistic grain boundary pore shape, a cross-section formed by closely packed uniform rods, to represent the flow channel cross-sections in sandstone rocks, leads to good agreement between the simulated and measured electrical resistivity and capillary pressure. Tsakiroglou and Fleury [15] used pore network simulations to study the synergistic effect of geometrical, topological and fractal properties of the pore space on resistivity index curve over high, medium and low Sw.

In the present work, a pore network model is used to study the effect of input parameters on the prediction of capillary pressure, resistivity index and gas/oil relative permeability of homogeneous media. The investigated rock is a Fontainebleau sandstone rock with a porosity of 22.5% and gas permeability of 1963 mD. The gas/oil relative permeabilities are calculated in the numerical pore networks and compared to experimental curves. The key parameters of the model giving a representative pore network are determined. The resistivity index curve is then calculated. The so-called 'non-Archie' behavior is obtained numerically as observed in experiments. The possibility to extend this work to dual-porosity rocks is also demonstrated and some preliminary simulation results are presented.

PORE-SCALE MODELING

Network model construction for single porosity

The network model developed in this work respects the converging-diverging nature of pores, the pore space multiple connectivity, the pore-size distribution and the existence of pore space angulosities. The pore space is simulated as a three-dimensional cubic lattice formed by pore-bodies (nodes) interconnected by pore-throats (bonds). More details on the model characteristics and construction are provided in a previous paper (Laroche and Vizika [8]).

In the simulations presented here each pore-body is assumed to be accessible by six pore-throats of identical inscribed diameter *d*. This implies that pore-throats, which link by definition two pore-bodies, do not have a constant section and are defined by two diameters. The aspect ratio, *AR*, relates the pore-body diameter *D*, to the pore-throat diameter *d*. The pore-body volume is assumed to be proportional to the pore inscribed diameter *D* to an exponent, λ_p, following the relationship $V_p(D) \sim D^{\lambda p}$. This empirical approach has been used by many authors to represent the relationship between radius and volume for real pores (Heiba et al., [7]; Fenwick and Blunt [5]). More precisely:

$$V_p(d) = c_p \, \overline{D}^{(3-\lambda_p)} AR^{\lambda_p} d^{\lambda_p} , \qquad (1)$$

where c_p is a coefficient around unity and $\overline{D}$ the average pore-body diameter.

Similarly the pore-throat length is assumed to be correlated to the pore-throat radius according to three different scenarios: (1) $\lambda_t = 0$, the pore-throat length is constant and defined as $l_t(d) \sim (L-\overline{D})$, where L is the lattice periodicity length (node-to-node distance) ; (2) $\lambda_t = 1$, the pore-throat length is proportional to the pore-throat radius: $l_t(d) \sim (L-\overline{D}) \cdot d/\overline{d}$; (3) $\lambda_t = -1$, the pore-throat length is inversely proportional to the pore-throat radius: $l_t(d) \sim (L-\overline{D}) \cdot \overline{d}/d$ or alternatively $l_t(d) \sim (L-D) \sim (L-AR \cdot d)$. The prefactor used in these relationships defining the pore-throat length is c_t, a coefficient around unity. For given λ_p and λ_t, the prefactors c_p, c_t and the periodic length L have to be adjusted to reproduce the rock permeability, porosity and formation factor obtained through experimental determination.

Pore size distribution from mercury invasion capillary pressure curve

The useful information to be extracted from the mercury invasion curve for the construction of the network model is the number based throat size frequency.

To determine the number based throat size frequency certain assumptions on the pore geometry need to be made: (i) radii r calculated from the capillary pressure values correspond to the threshold radii to invade pore bodies of radius $R \sim r$; (ii) the elementary volume of a pore (a node and its throats) follows $v(r) \sim r^{\lambda p}$. If $<v>$ is the average elementary volume of a pore, verifying $<v> \sim <r^{\lambda p}>$, the number based frequency is given by:

$$F_n(r) = \left| \frac{<v>}{v(r)} dS \right| \tag{2}$$

As already mentioned, no information is directly extracted from the mercury invasion P_c curve concerning the pore-body size distribution. However, if the pore-body size is assumed to be proportional to its threshold radius $R \sim r$ through the aspect ratio AR, the pore-throat size distribution will determine the pore-body size distribution automatically.

Calculation of the network petrophysical parameters

Network invasion methodology

Capillary pressure curve is obtained by simulating quasi-static displacement where an increasing pressure is applied on the injected fluid, while the pressure of the fluid in place is kept constant. During quasi-static displacement, viscous pressure gradients are negligible, and the pressure of each phase is constant everywhere within the network. Expressions to evaluate the saturations in each unit element can be found elsewhere (Laroche and Vizika [8]).

Relative Permeability and resistivity index calculation

The absolute permeability K of the network is found from Darcy's law when the network is fully saturated with a single phase. The two-phase relative permeability curves are calculated at each step of the two-phase quasi-static displacements when capillary equilibrium is reached. Flow within each phase is simulated by applying a macroscopic pressure gradient ΔP across the network of length L_{net}. It is found by solving for the local pressure by imposing mass conservation at every pore body. If Q_α is the flow rate,

μ_α the viscosity of phase α, K the permeability and A the cross-section of the porous medium, the relative permeability of phase α is calculated as:

$$K_{r\alpha} = \frac{Q_\alpha \mu_\alpha L_{net}}{AK\Delta P} \tag{3}$$

The electrical analogy to absolute permeability is the formation factor

$$FF = \frac{\sigma_w}{\sigma_0} \tag{4}$$

where σ_0 is the electrical conductivity computed at 100% water saturation and σ_w is the electrical conductivity of bulk water. The network conductivity is given by Ohm's law

$$\sigma_0 = \frac{I.L_{net}}{A.\Delta V} \tag{5}$$

where ΔV is the imposed voltage and I is the total current intensity. The equations are solved for the potential at each node, imposing current conservation at every pore body. The electrical resistivity index IR is given by

$$IR = \frac{\sigma_0}{\sigma_t} \tag{6}$$

where σ_t is the electrical conductivity at a given water saturation.

The tortuosity (τ) expresses the path length of the electrical current and reflects the manner in which the pores are interconnected. If ϕ is the porosity, the tortuosity is given by

$$\tau = (FF\Phi)^{1/2} \tag{7}$$

Potential and pressure field calculation

The calculation of the fluid flow of each phase spanning the network and the calculation of the electrical current in the aqueous phase each use the same electrical analog. Electrical and hydraulic conductivities are used to solve for the potential and pressure field, respectively.

The local electrical conductance, g_{eij}, relates the local electrical flux, I_{ij}, between two neighboring pores, ij, to the potential difference between these two pores:

$$I_{ij} = g_{eij}\,(U_i - U_j) \tag{8}$$

This equation only applies to the electrically conductive phase, i.e. the water phase. Similarly, for laminar flow the relationship between pressure drop and fluid flux in the network is linear. The local flow rate for a given phase α between pore i and neighboring pore j is defined as:

$$q^\alpha_{ij} = g^\alpha_{ij}\,(P^\alpha_i - P^\alpha_j) \tag{9}$$

where g^α_{ij} is the local hydraulic conductance of the particular fluid α, in bulk phase or film phase between pores i and j. In each pore i, the continuity equations are verified. Electrical and hydraulic problems are reduced to a system of linear algebraic equations, the solution of which gives respectively the electrical potential and the pressure of each phase in the pores.

Hydraulic and electrical conductance

The hydraulic conductance of a non-wetting phase in a pore segment of length l is defined using Poiseuille's law and an effective radius r_{effNW} for the flow:

$$g_{NW} = \frac{\pi \cdot r_{effNW}^{4}}{8\,\mu_{NW} \cdot l} \qquad \text{with} \qquad r_{effNW} = \sqrt{\frac{A_{NW}}{\pi}} \tag{10}$$

where A_{NW} is the cross-sectional area occupied by the non-wetting phase.

The hydraulic conductance of the wetting phase is approximated by an expression derived by Ransohoff and Radke [12]:

$$g_W = \frac{A_W\, r^2}{\beta_W\, \mu_W\, l} \tag{11}$$

where A_W is the cross-sectional area occupied by the wetting phase, r is the radius of curvature of the interface and β_W is a dimensionless resistance factor. Quantitative expression for the hydraulic conductance of the different phases can be found in previous work for the angular geometry (Laroche and Vizika [8]).

The electrical conductance of the water phase in a pore segment of length l is given by:

$$g_e = \sigma_w \frac{A_w}{l} \tag{12}$$

where A_w is the cross-sectional area occupied by the water phase. The calculation of the effective electrical conductance between two neighboring pores, takes into account the water phase occupancy in the different pore segments (pores and throat).

Dual pore-network modeling

The network model approach is applied at two scales and is illustrated schematically in Figure 1. The model combines transport properties of the primary porosity (capillary pressure and relative permeabilities of the matrix which is considered homogeneous) with the pore network modeling approach used to simulate the secondary porosity (vugs or fractures).

A dual-porosity medium is characterized by a bimodal pore-throat radii distribution. The larger pore-throat radii are used to build a three-dimensional lattice of pores and throats representing the behavior of the secondary porosity as described above (the network may be partially disconnected). These pores and throats are surrounded by a matrix with known properties (porosity, absolute permeability, capillary pressure and relative permeability curves). Matrix permeability K_m and porosity Φ_m may be spatially distributed within the 3-D lattice. In this paper, we assume for simplicity that matrix properties are uniform.

Calculation of the dual pore-network petrophysical parameters

Dual pore-network invasion methodology

The primary drainage in dual-porosity rocks is simulated using the invasion percolation model described above with the following modification. The capillary

pressure required for the non-wetting phase invasion into a pore or throat may be determined by either its size r, or the breakthrough capillary pressure of the matrix $\{Pc^0\}_m$. This may be expressed as

$$Pc^0 = max[Pc(r), \{Pc^0\}_m] \quad (13)$$

where $Pc(r)$ is the threshold pressure of the throat or pore. When the externally applied pressure exceeds $\{Pc^0\}_m$, the matrix will be invaded by the non-wetting phase and all pores/throats from the secondary porosity become accessible through the matrix. Therefore, the presence of the matrix allows isolated pores/vugs to be invaded. Accessible pores/throats are invaded if the externally applied pressure exceeds their threshold pressure $Pc(r)$.

Average petrophysical parameters

The total porosity Φ of a dual pore-network is calculated from the primary Φ_m and secondary porosity Φ_s:

$$\Phi = \Phi_s + \Phi_m.(1- \Phi_s) \quad (14)$$

Similarly, the average wetting phase saturation Sw is calculated, for each applied capillary pressure Pc, from the primary Sw_m and secondary porosity wetting phase saturation Sw_s:

$$\Phi .Sw = \Phi_s.Sw_s + \Phi_m.(1- \Phi_s).Sw_m(Pc) \quad (15)$$

The calculations of the fluid flow and current intensity are done in a similar way considering that primary and secondary porosity systems are parallel. The effective electrical and hydraulic conductances are given as the sum of the local conductances of each system.

The effective hydraulic conductivity g^α and electrical conductance g_e are calculated for each applied capillary pressure Pc knowing the matrix capillary pressure:

$$g^\alpha = g^\alpha_s + g^\alpha_m(Sw_m(Pc)) \quad (16)$$

$$g_e = g_{es} + g_{em}(Sw_m(Pc)) \quad (17)$$

where g^α_s and g_{es} are the conductivity and electrical conductance of the secondary porosity. The matrix hydraulic conductivity $g^\alpha_m(Snw_m(Pc))$ is obtained from relative permeability functions using eqn (3) and the matrix electrical conductance $g_{em}(Sw_m(Pc))$ by:

$$g_{em}(Sw_m(Pc)) = \sigma_w [FF_m IR_m(Sw_m(Pc))]^{-1} (1- \Phi_s) lx.ly/lz \quad (18)$$

This relationship can also be expressed using the general Archie relationship:

$$g_{em}(Sw_m(Pc)) = \sigma_w \Phi^{-m_m}.Sw_m^{n_m}(Pc) (1- \Phi_s) lx.ly/lz \quad (19)$$

where n_m is the matrix saturation exponent, m_m is the matrix cementation exponent, and σ_w the bulk water conductivity.

RESULTS AND DISCUSSION

The investigated rock is a Fontainebleau sandstone with ϕ =22.5% and K=1963 mD. The sample is a well sorted sandstone, with an average grain size of 250µm (Bourbie and Zinszner [2]). The 3D geometry and connectivity of the pore space of several Fontainebleau samples ranging from 8 to 22% porosity has been previously extracted

from 3D synchrotron X-ray computed microtomographic images, using computer analysis (Lindquist et al. [9]). These 3D images have a uniform resolution of just under 6µm in all three directions. The measured data indicate an overall increase in coordination number and shortening of pore channel length with increasing porosity. The average coordination number ranges from 3.4 to 3.8; the average channel ranges from 200 to 130µm. Average effective throat radius varies from 18 to 22µm, assuming circular area, while average pore volume remains unchanged around 0.0004 mm^3 (average effective pore radius remains unchanged around 45-50µm).

Capillary pressure curves

It is interesting to compare this detailed description of the pore space obtained by 3D images to the different pore space geometry scenarios obtained by applying our methodology for interpreting mercury porosimetry curves.

As described above, the exponent λ_p for the pore volume determination is used to extract the pore-throat size distribution from mercury porosimetry curves. Different scenarios have been tested for λ_p varying between 0 and 2, providing different pore-throat size distributions. The calculated pore-throat radius distributions in terms of frequency $F_n(r)$, obtained for the different scenarios described in Table 1, are shown on Figure 2.a.

The scenarios (Run # 1 to 3) considering constant pore volume behind each throat (λ_p = 0) lead to a very good agreement between the experimental and simulated Pc curves. However, as it is shown in Figure 3.a and 3.b, it is impossible with these scenarios to reconcile the calculated gas/oil relative permeability curves to the experimental ones (high value of the calculated K_{rg}). A correlation between pore-throat length and radius (λ_t = -1, 0, 1) does not affect the capillary pressure results, as seen on Figure 2.c. On the other hand, the calculated formation factor and the saturation exponent n are lower when the pore-throat length is proportional to its radius (λ_t = 1).

The scenario that assumes a weak correlation between pore volume and pore-throat radius, λ_p = 1, is not treated here. The unrealistic high proportion of very small throats (97% below 1µm, see Figure 2.a and 2.b) obtained in with this scenario does not satisfy either porosity, permeability or the capillary pressure curve using any of the chosen parameters (C_p, C_t, L). The forth and fifth scenarios are aimed at improving the agreement between the experimental and simulated curves, by applying the correlation exponent λ_p to throats above 5µm, and considering that small throats (below 5µm) are connected to pores of constant volume. The proportion of small throats can be varied in order to vary their weighting within the overall porous volume.

In the fourth scenario, pore volumes are assumed to be weakly correlated to throat radius (λ_p = 1), except for small throats, below 5µm, which are connected to constant pore volume. In that 4th scenario, a proportion of 30% of small throats has to be considered in order to satisfy the capillary pressure curve. The fifth scenario assumes a stronger correlation between pore volume and pore-throat radius, λ_p = 2. The capillary pressure curve is satisfied if a proportion of 17% of small throats (below 5µm) is assumed. It is seen on Figure 2.c that the agreement between simulated and experimental Pc curves is slightly poorer in that latter case, but the deviation is observed in the region

of very low capillary pressure values, which are artificially stretched on this figure due to the use of logarithmic coordinates. Both scenarios (4 and 5) lead to similar porosity and permeability values, but different formation factor (Table 1). The 5th scenario seems more consistent with the expected value of formation factor around 15, for a sample with 22% porosity.

The measured pore size distribution obtained by Lindquist et al. from the analysis of microtomographic images is also shown on Figure 2.b for comparison purposes. It has to be noted that this measured distribution only accounts for throat size above the resolution of the X-ray synchrotron (typically ~5µm). It makes sense to compare this measured distribution to the calculated distributions obtained by applying a "cut-off" at 5µm radius (run #4 and 5). It is seen from Figure 2.b that the best agreement is obtained for the scenario where λ_p = 2 for throat radius above 5µm. This scenario corresponds to run #5 which gave the best prediction in terms of petrophysical parameters such as porosity, permeability and formation factor. The coordination number has also been calculated on the constructed network in order to compare with the measured coordination number on the microtomographic images. For comparison purposes an average modified coordination number is calculated which takes into account only the throats of radius above the "cut-off" value, i.e. 5µm. The calculated value is <Z> = 4 for run #5. This is in very good agreement with the measured value of Z = 3.75, which was obtained in the analysis of the microtomographic images of the sample with 22% porosity.

Relative permeability curves

The gas/oil relative permeability has been calculated for a network constructed using the pore-throat size distribution obtained with the different scenarios described in Table 1. The calculated permeability has been obtained by simulating a gas invasion in a network containing Swi = 23%. The irreducible water saturation is first established by simulating an oil invasion in a network fully saturated with water. The results are presented in Figure 3 both in logarithmic and linear coordinates. The experimentally measured values (steady-state, positive spreading coefficient, Swi around 20%, from Kalaydjian et al. [6]) are also given.

Figures 3.a and 3.b show how relative permeabilities are affected by the correlation between the pore-throat length and radius (λ_t = -1, 0, 1. i.e. pore-throat length is inversely proportional, constant and proportional to its radius, respectively). The corresponding scenarios are run # 1, 2 and 3, where constant pore volume is considered behind each throat (λ_p = 0). It is clearly shown that oil and gas relative permeabilities have an opposite behavior with λ_t. When the λ_t value increases (-1, 0, 1), the oil relative permeabilities increase whereas the gas relative permeabilities decrease. The network constructed with λ_p = 0 (Run #1 to 3) leads to a very good agreement between the experimental and simulated Pc curves at all λ_t values. However, it was impossible to reconcile calculated gas/oil relative permeability curves to the experimental ones (high value of the calculated K_{rg}). Figures 3.c and 3.d show the relative permeability results for two scenarios (correlation between pore-throat and pore-body size, run #4 and 5), to be well

representative of the considered rock. A satisfactory agreement between simulated and experimental curves is obtained for both scenarios (run #4 and 5).

Resistivity index curves

Resistivity index (*IR*) curves have been calculated by simulating oil invasion in water-wet networks which are fully saturated with water. Networks constructed using the pore-throat size distributions obtained using the scenarios in Table 1 are considered to study the effect of λ_p and λ_t on the *IR* curves.

The saturation exponents obtained with the fourth and fifth scenario are equal to 1.94 and 1.91, respectively. They are comparable to the commonly measured exponents in sandstones, which are in the range of 1.8-2. The scenarios which assume constant pore volume behind each throat (λ_p=0; Run #1 to 3) lead to a slightly higher value of the saturation exponent. The first and second scenario, where the pore-throat length is assumed to be inversely proportional to its radius (λ_t=-1) and constant (λ_t=0), respectively, yield a higher saturation exponent, i.e. 2.82. The trend is the same for the formation factor, the cementation exponent and the tortuosity factor (Table 1). It is seen that both *n* and *IR* (Figure 4) are affected by the pore size distribution. The saturation exponent is clearly a decreasing function of the pore shape factor (λ_p). This behavior is consistent with previously reported results (Tsakiroglou and Fleury [15]). It is also seen that a deviation from the straight line is observed around Sw=0.1, where *IR* shifts towards higher values. This deviation from Archie's law has been confirmed experimentally for certain types of rocks (Diederix [4]; Swanson [14]).

The effect of the pore structure on IR is shown on Figure 5. The results presented in Figure 5 are obtained by constructing the pore network using the pore size distribution of run #2 described in Table 1. Different parameter values lead to different pore structures even if the pore size distributions are identical. Pc and IR results are presented in Figure 5. It is observed that both resistivity index and saturation exponent depend strongly on the pore space geometry and wettability characteristics. The simulations demonstrated that several situations give important deviations from Archie's law. Upward going resistivity index curves indicate a disconnection of the conductive phase, water. This disconnection may occur even at relatively high water saturations in oil-wet porous media. In water-wet rock, this effect appears at much lower water saturations (<3%). Downward bending resistivity index curves are observed in structures with correlated pore-body and pore-throat sizes. The phenomenon is amplified when the aspect ratio increases. This can be easily explained since the higher the aspect ratio, or the stronger the pore-body/pore-throat correlation, the higher the non-wetting phase saturation at the same pressure level. But same pressure level at low wetting phase saturation means similar wetting film thickness and consequently similar resistivity index.

Dual-network calculation

The carbonate rock (ϕ=33.8% and *K*=115 mD) with bimodal porosity structure consisting of a fine-grained matrix and both well connected and isolated (communicating only through the matrix) macropores (Moctezuma et al. [11] and Békri et al. [1]), was used in this study. For such rock, each porosity system is treated separately and the

average macroscopic quantities (*Kr*, *Pc* and *IR*) are calculated using the dual network approach. More details on the network construction and the used scenario can be found in previous work (Moctezuma et al. [11] and Békri et al. [1]). Preliminary simulations show that Archie's law roughly holds for a large range of saturations (Figure 6). However, the saturation exponent would be clearly above 2.

CONCLUSION

Network modeling has been used to interpret mercury porosimetry data and to construct pore networks which satisfy the capillary and standard petrophysical properties of real rocks. Gas/oil relative permeabilities in the presence of irreducible water have been calculated and compared to experimentally determined curves. Resistivity index curves have also been calculated and a sensitivity analysis to the network parameter values was performed. An extension to dual-porosity rocks and some preliminary simulation results were presented. It has been seen that the geometrical parameters of the network and the wettability condition dramatically affect transport and electrical property functions.

A good agreement is obtained between experimental and calculated relative permeabilities for correlated pore-body and pore-throat sizes, while for uncorrelated pore-body and pore-throat populations calculated *Kr* overestimate the experimentally obtained values.

The "non-Archie" behavior of the *IR* curves was explained in terms of rock wettability and pore structure characteristics. Oil-wet porous media have high saturation exponents and early (at higher water saturations) upward bending resistivity index curves. Water-wet rocks give lower saturation exponents and upward bending curves at much lower water saturations (<3%). Correlated pore-body and pore-throat sizes as well as high aspect ratios can explain the downward bending *IR* curves that have been often observed in carbonate rocks.

REFERENCES

1. Békri S., Nardi C. and Vizika O., “Effect of wettability on the petrophysical parameters of vuggy carbonates; network modeling investigation”, SCA2004-25, *International Symposium of the Society of Core Analysts*, Abu Dhabi, UAE, 2004.
2. Bourbie T. and Zinszner B., “Hydraulic and acoustic properties as a function of porosity in Fontainebleau sandstone”, *Journal of geophysical research*, (1985) **90** ,11,524-11,532.
3. Dicker A. I. M. and Bemelans W. A., “Models for simulating the electrical resistance in porous media”, 25th *SPWLA Ann. Logg. Symp.*, New Orleans, 1984.
4. Diederix K. M., “Anomalous relationships between resistivity index and water saturations in the rotliegend sandstone (The Netherlands)”, *23rd SPWLA Ann. Logg. Symp.*, Corpus Christi, TX, (1982).
5. Fenwick D.H. and Blunt M.J., “Three-dimensional modeling of three-phase imbibition and drainage”, *Adv. Water Resources*, (1998) **21**(2), 121-143.

6. Kalaydjian F., Vizika O., Moulu J. C. and Munkerud P. K., "The role of wettability and spreading in gas injection processes under secondary conditions", Geological Society- Special Publication, (1995) **84**, 93-71.
7. Heiba A.A., Sahimi M., Scriven L.E. and Davis H.T., "Percolation theory of to-phase relative permeability", *SPE Reservoir Engineering*, (1992) **7**, 123-132.
8. Laroche C., Vizika. O., "Two-Phase Flow Properties Prediction from Small-Scale Data Using Pore-Network Modeling", *Transport in Porous Media*, (2005) **61,** N1, 77-91.
9. Lindquist W.B., Venkatarangan A., Dunsmuir J. and Wong T., "*Pore and throat size distributions measured from synchrotron X-ray tomographic images of Fontainebleau sandstone*", *Journal of geophysical research*, (2000) **105**(B9) ,21,509-21,527.
10. Man H.N. and Jing X. D., "Pore network modelling of electrical resistivity and capillary pressure characteristics", *Transport in Porous Media*, (2000) **41**, 263-286.
11. Moctezuma A., Békri S., Laroche C. and Vizika O., "A dual network Model for relative permeability of bimodal rocks application in a vuggy carbonate", SCA2003-94, *International Symposium of the Society of Core Analysts*, Pau, France, 2003.
12 Ransohoff T. C. and Radke C. J., "Laminar flow of a wetting liquid along the corners of a predominantly gas occupied non circular pore", *J. Coll. Interface Sci.*, (1988) **121**, N2.
13. Sahimi, M., "Flow phenomena in rocks: from continuum modeles to fractals, percolation, celluar automata and simulated annealing", *Rev. Mod. Phy.* (1993) **65**, 1393-1534.
14. Swanson B. F., "Microporosity in reservoir rocks - its measurement and influence on electrical resistivity", 26th *SPWLA Ann. Logg. Symp.*, Dallas, Texas, 1985.
15. Tsakiroglou C. D. and Fleury M.: "Pore network analysis of resistivity index for water-wet porous media", *Transport in Porous Media*, (1999) **35,** 89-128.
16. Wang Y. and Sharma M. M., "A network model for the resistivity behavior of partially saturated rocks", 29th *SPWLA Ann. Logg. Symp.*, San Antonio, Texas, 1988.

Table 1: Different scenarios tested to describe the considered Fontainebleau sandstone rock

Run scenarios	Φ %	K (mD)	FF	m	τ	<Z>	n	L	$<D_p>$	$<d_t>$	$<l_t>$
Run #1 : AR = 3.1 $\lambda_p = 0$; $c_p = 1.97$ $\lambda_t = -1$; $c_t = 1.86$	22.5%	1963	33	2.34	2.72	5.0	2.82	290	127	40	233
Run #2 : AR = 3.1 $\lambda_p = 0$; $c_p = 1.94$ $\lambda_t = 0$; $c_t = 1.64$	22.6%	1968	32	2.33	2.69	5.0	2.82	290	127	40	205
Run #3 : AR = 3.1 $\lambda_p = 0$; $c_p = 1.85$ $\lambda_t = 1$; $c_t = 1.5$	22.5%	1961	30	2.28	2.61	5.0	2.35	290	127	40	188
Run #4 : AR = 3.1 $\lambda_p = 1$; $c_p = 1.58$ 30% r<5µm $\lambda_t = 0$; $c_t = 1.1$	22.5%	1961	24	2.13	2.31	2.4	1.94	190	89	28	86
Run #5: AR = 2.1 $\lambda_p = 2$; $c_p = 1.42$ 17% r<5µm $\lambda_t = 0$; $c_t = 1.15$	22.5%	1959	17	1.90	1.96	4.0	1.91	150	59	28	81

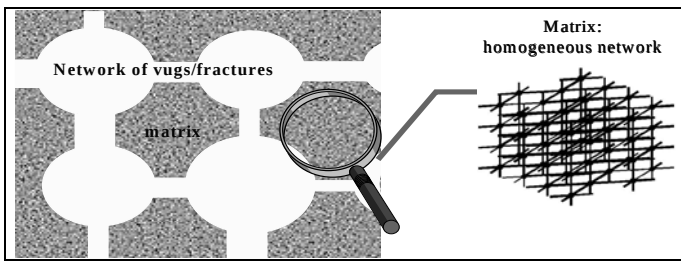

Figure 1. Schematic depiction of a dual-network

(a)

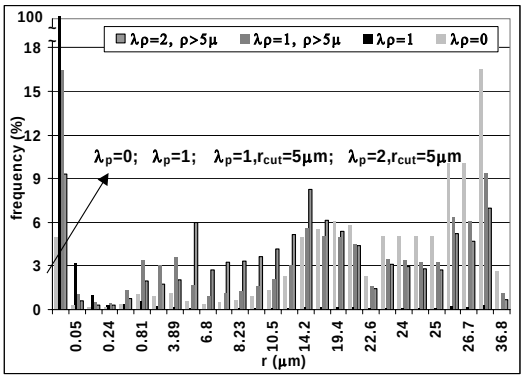

(b)

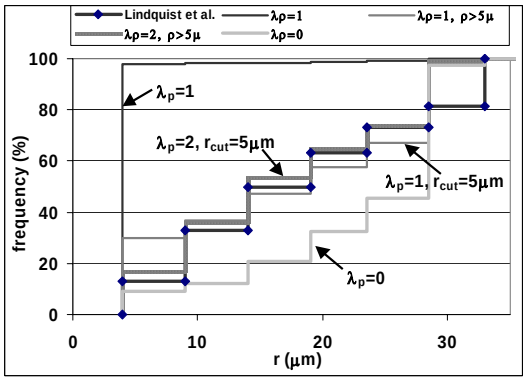

(c)

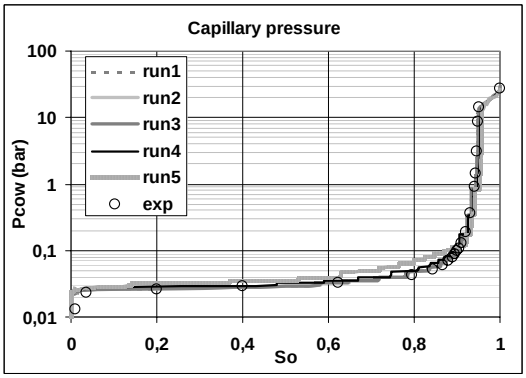

Figure 2. **(a)** Pore-throat radius distributions obtained with different λ_p scenarios; **(b)** Cumulative pore-throat radius distributions and comparison between distributions obtained with different λ_p scenarios and measured distribution from analysis of the microtomographic images by Lindquist et al.; **(c)** Comparison of capillary pressure curves obtained experimentally and by simulations with different pore space geometry scenarios.

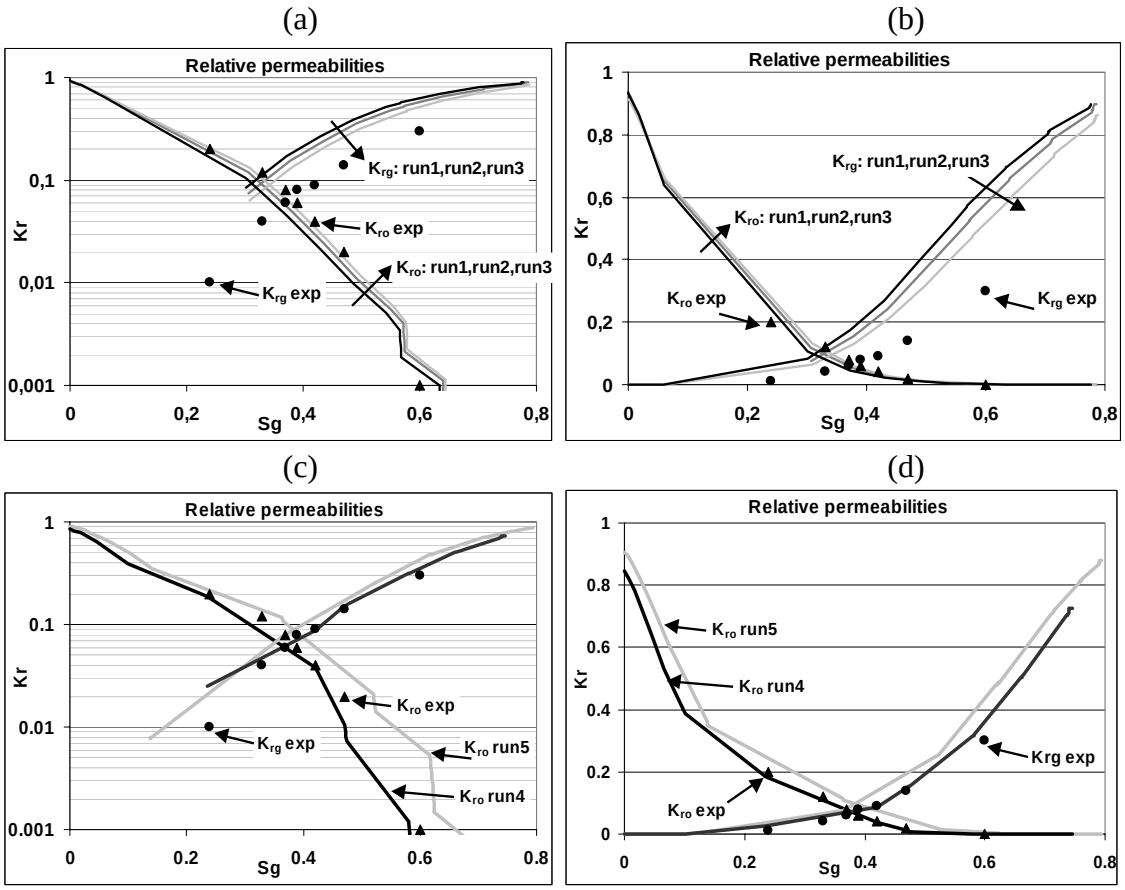

Figure 3. Comparison of gas/oil relative permeability curves Krog = f(So) obtained experimentally and by simulations at irreducible water saturation (around 20%) with different pore space geometry scenarios. Experimental data: steady-state Krog for positive spreading coefficient, from Kalaydjian et al.[6].

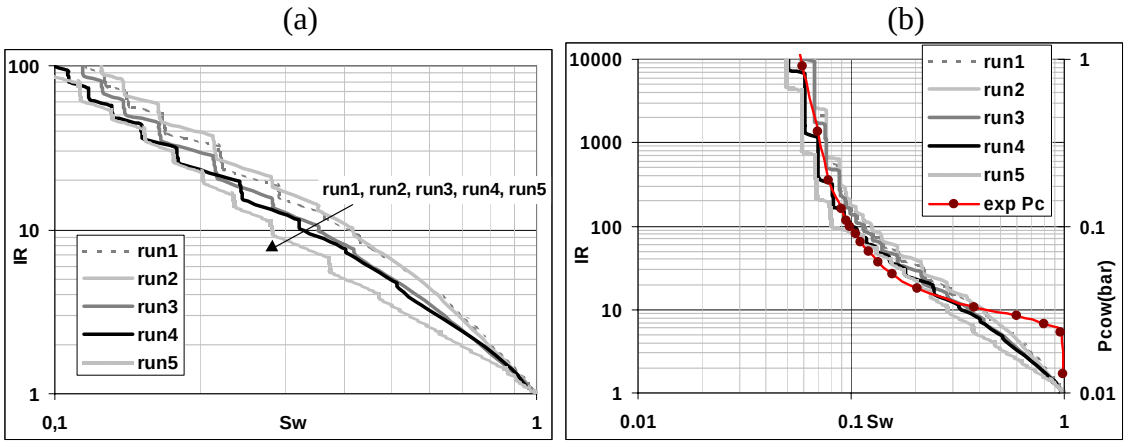

Figure 4. Simulated resistivity index curves with different pore space geometry scenarios described in Table 1 and the corresponding Pc curve.

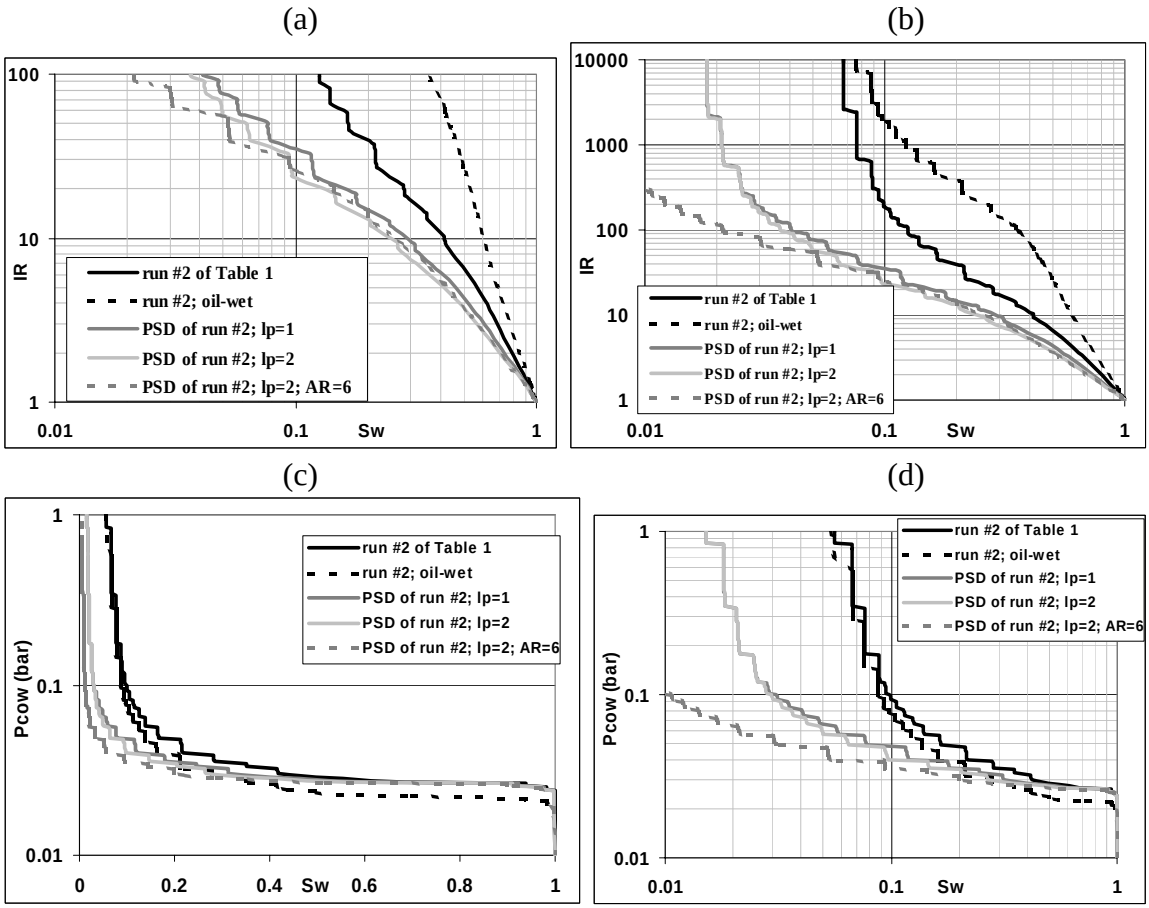

Figure 5. Simulated resistivity index curves (a, b) and capillary pressure curves (c, d) for network constructed using the pore size distribution of run #2 described in Table 1. Different parameter values, which lead to different pore structures, were used.

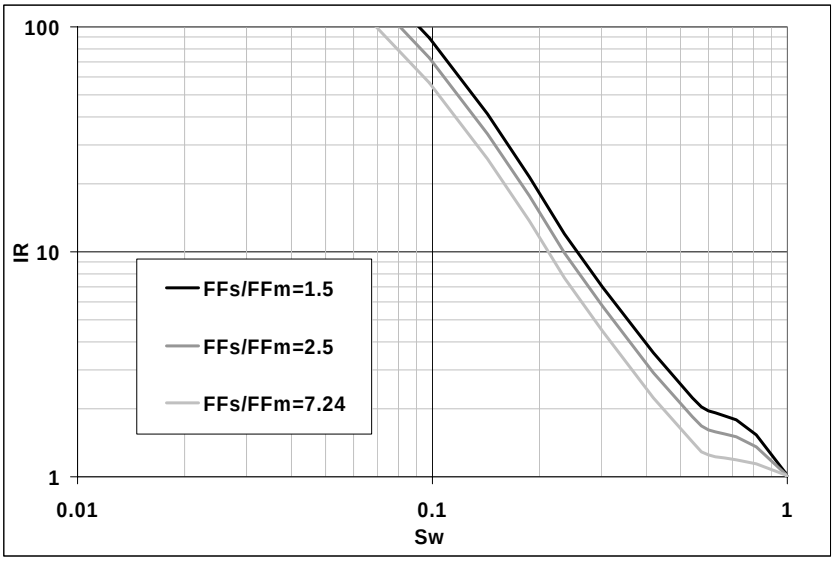

Figure 6. Simulated resistivity index curves for dual-porosity rocks. The carbonate rock, the pore size distribution and the numerical parameters used here are those described in Moctezuma et al. [11] and Békri et al. [1].